# **CONFERENCE PRE-PRINT**

# IMPACT OF TRANSIENT HEAT LOADS ON THE DETACHED MAST UPGRADE SUPER-X DIVERTOR

R. Scannell, S. Leigh, Z. Huang, J. Harrison, S. Silburn, P. Ryan, S. Henderson, N. Lonigro, D. Moulton, S. Blackmore and the MAST-U Team UKAEA, Culham Campus, Abingdon, UK Email: rory.scannell@ukaea.uk

J. Flanagan University of Liverpool, Liverpool, UK

#### **Abstract**

The MAST Upgrade Super-X divertor protects plasma-facing components from heat fluxes during steady-state operation and transient events. This paper examines the buffering of heat loads from sawtooth events with energies of  $\Delta W_{\rm Sawtooth} \approx 2$ –8 kJ in lower single null plasmas. We investigate the impact of deuterium and nitrogen gas on mitigating these transients. Increasing  $D_2$  gas pressure buffers transients with energies up to 6 kJ, reducing peak heat flux by approximately 0.17MW/m²/Pa. Together, the variation in transient energy and deuterium gas pressure accounts for 70–80% of the variation in transient burnthrough, as measured by infrared thermography heat flux and Fulcher band emission. A small subset of larger sawtooth transients ( $\Delta W_{\rm Sawtooth} \approx 6$ –8kJ) falls outside this trend and shows much higher target heat fluxes suggesting depletion of the neutral gas buffer. A comparison between Super-X and conventional divertor configurations shows that the Super-X configuration experiences significantly lower peak heat fluxes for similar  $\Delta W$ , consistent with expectations based on divertor geometry. For transients with energies  $\Delta W_{\rm Sawtooth} \lesssim 6$ kJ,  $N_2$  seeding yields a larger reduction in peak heat flux, about 4.1 MW/m²/Pa, and complete buffering of sawtooth transients at high nitrogen pressure. Direct divertor  $T_e$  measurements indicate quiescent inter-transient temperatures of 1eV, rising to 6–8eV during sawtooth transients, with profiles showing decreasing  $T_{e,div}$  and increasing  $n_{e,div}$  in the last 0.4m poloidally from the target. In cases where divertor heat loads exceed  $q_{\perp} > 2$ MW/m², we observe  $T_{e,div}$  exceeding 10eV. These measurements are compared to modelling using the ReMKiT1D code for a range of transient  $\Delta W$  and recycling timescales, the results of this modelling indicates target recycling plays a significant role in determining divertor parameters during transients.

## 1. INTRODUCTION, EXPERIMENTAL SET-UP AND DIAGNOSTICS

The reliable handling of transient heat loads remains a key challenge for the next step of magnetically confined fusion devices. Plasma instabilities such as sawtooth crashes and edge localized modes (ELMs) release stored thermal energy, delivering intense bursts of heat flux to plasma-facing components (PFCs) [1]. In future reactor-scale devices, transient heat loads must be prevented where possible or mitigated, for example by impurity gas puffing, where prevention is not possible. The MAST-U experiment was designed, amongst other things, to explore advanced divertor configurations, in particular the Super-X divertor (SXD) [2]. By extending the outer divertor leg and increasing the connection length, the SXD reduces heat and particle flux at the target by spreading it over a larger area [3]. These geometry improvements allow for easier detachment and mitigate both steady-state and transient power loads. Additionally, the Super-X configuration allows a high neutral pressure in the divertor which increases the exhaust power dissipation before the strike point [4]. Taking all these factors into account, the Super-X then provides a potential power handling solution for future fusion power plants [5]. For STEP, the maximum long term heat load has been quoted as 10 MW/m<sup>2</sup> and 20MW/m<sup>2</sup> for transient heat loads[6], which are similar to the ITER requirements [7]. ELMs transients have been a particular focus of concern and their impact machine survivability has been an active area of research [8]. A recent paper on transient heat loads on MAST-U focused specifically on ELMs [9], this current paper extends this analysis to Sawteeth. Experimentally, techniques such as  $N_2$  seeding have been used to increase radiative power dissipation, and thereby reduce peak target heat flux [10]. The plasma scenarios analyzed for this paper consisted of lower single null, L-mode plasmas with plasma currents of  $I_p \approx 0.75 \mathrm{MA}$  and  $B_T \approx 0.6$  T on axis. Sawtooth instabilities were naturally present in these discharges, releasing transient energies in the range  $\Delta W_{\rm sawtooth} \approx 2$ –8 kJ, determined from the change in stored energy from equilibrium reconstruction. The plasmas had only a single on-axis neutral beam with typical injected heating power  $P_{NBI}$ =1.6MW and did not

deploy the *off-axis* beam which would have de-stabilised the sawteeth making them more frequent and smaller in magnitude. All discharges studied as part of this work were in L-mode, which was ensured by application of low field side rather than high field side gas. While the divertor gas was varied, the low field side main chamber *fuelling* gas was constant for all discharges. This paper uses the DART tool (Detachment Analysis with Reduced modelling Tools)<sup>1</sup>, [6] which can infer the neutral pressure at various locations. Divertor heat fluxes were measured by a infrared (IR) thermography system viewing the outer target. The IR data were analyzed using a surface heat transport code to infer the perpendicular heat flux profiles during and between sawtooth crashes. Divertor Thomson scattering [11] (DTS) provide local measurements of  $T_{e,div}$  and  $n_{e,div}$ , characterizing the divertor plasma response to transient events. An Ultra Fast Divertor Spectroscopy (UFDS) diagnostic which looks at Fulcher band emission, indicative of the detachment front location, across several lines of sight along the Super-X divertor is also used.

# 2. $D_2$ AND $N_2$ GAS SCANS

Deuterium gas injection into the divertor chamber was varied from 0 to  $1.2 \times 10^{22}$  particles/s over eight pulses. Across the deuterium gas pressure scan, no systematic trend was observed in the amplitude of sawtooth energy losses. However, as the gas pressure increased, both the Target/Upstream Fulcher ratio and the peak IR-measured transient heat flux typically decreased. This behaviour indicates that raising the divertor  $P_{gas}$  can effectively reduce the peak heat loads from sawtooth transients, consistent with spectroscopic observations previously reported for ELM transient mitigation [9].

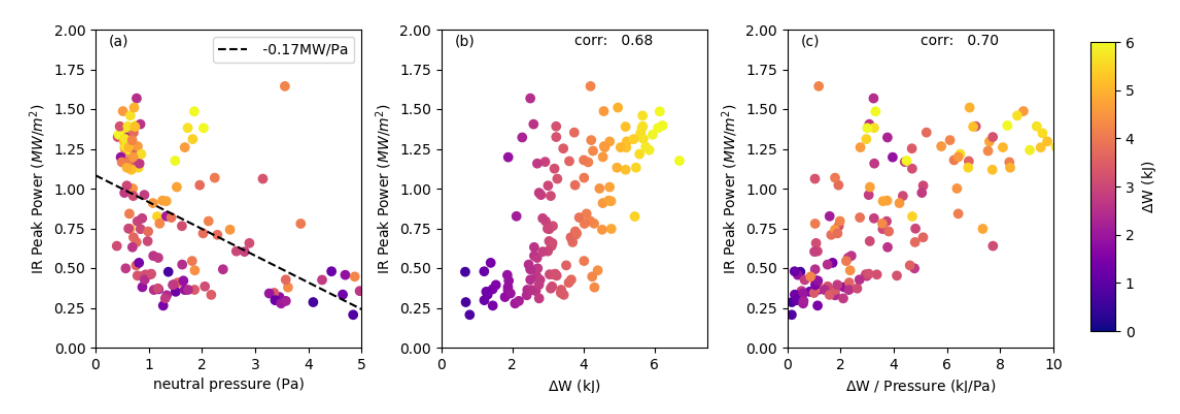


FIG. 1. Statistical analysis of 130 sawtooth transient events with  $q_{\perp} < 2$ , MW/m<sup>2</sup>. Peak IR-measured divertor heat flux plotted versus (a) main divertor neutral gas pressure, (b) transient energy loss  $\Delta W$ , and (c) combined parameter  $\Delta W$ /Pressure.

The individual sawtooth transients identified in the discharges were analysed and compiled into a database, recording both the transient energy loss and the corresponding divertor neutral gas pressure for each event. In total, 138 sawtooth events were analysed; of these, 130 satisfy the condition  $q_{\perp} < 2$ , MW/m² and are presented in Figure 1. The figure shows the peak IR heat flux plotted against: (a) the divertor main chamber neutral pressure inferred from DART, (b) the transient energy loss  $\Delta W$ , and (c) the ratio  $\Delta W$ /Pressure. As shown in Figure 1(a), the peak IR heat flux decreases significantly with increasing neutral gas pressure, with a linear fit showing a reduction of  $0.17 \text{MW/m}^2/\text{Pa}$ . These results suggest that increasing divertor  $P_{gas}$  mitigates burn-through and peak heat loads during sawtooth transients. Conversely, Figure 1(b) shows that both the peak IR heat flux increases with the magnitude of the transient energy loss  $\Delta W$ . To investigate whether the variation in burn-through can be largely attributed to these two variables—transient energy and neutral gas pressure—Figures 1(c) plots the burn-through indicators against the combined parameter  $\Delta W$ /Pressure. Within this dataset, this combined parameter explains 70% of the variation in peak heat flux indicating that transient energy and neutral pressure together largely determine the divertor response to sawtooth events. The UFDS ratio, not plotted for brevity, showed very similar trends, 79% of the observed variation in the Target/Upstream Fulcher ratio, attributable to  $\Delta W$ /Pressure. The inter-transient  $q_{\perp}$  varies from 0.1-0.5 MW/ $m^2$  depending on neutral gas fuelling.

The full 138 sawtooth dataset is analysed on per transient basis and the results are shown in figure 2(a). To illustrate the difference between  $q_{\perp} > 2MW^2$  sawteeth, which we will term *High Burn Through Events* (HBE), and  $q_{\perp} < 2MW^2$  sawteeth, the two are displayed with different symbols. The Fulcher target intensity and IR peak power loads show that these *High Burn Through Events* despite being only slightly larger in terms of neutron loss

<sup>&</sup>lt;sup>1</sup>DART can be accessed through: https://github.com/shenders/dart

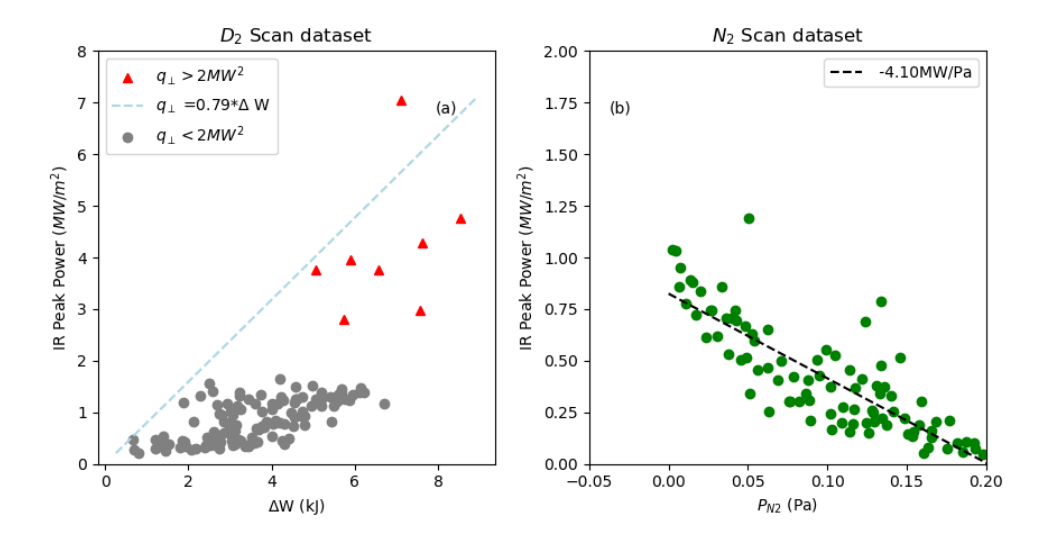


FIG. 2. Analysis of individual sawtooth transients (a)  $D_2$  gas scan separating *High Burn Through Events* (HBEs) from smaller events: peak IR vs. transient energy loss  $\Delta W$  (b)  $N_2$  gas scan: Peak IR heat flux vs. divertor neutral nitrogen pressure.

and  $\Delta W$ , are proportionately much larger in terms of impact on the divertor. This implies that these larger events are in a different physics regime compared to the lower amplitude sawteeth. The  $High\ Burn\ Through\ Events$  show very little relation to the scaling that was determined from the  $<2MW/m^2$  dataset. The HBEs are happening between 2.5-5Pa hence it is not believed that pressure is a determining factor but it is important to note as it contradicts the trend of increased buffering at higher neutral pressure from the  $<2MW/m^2$  dataset. Figure 2(a) shows that the  $High\ Burn\ Through\ Events$  are all higher energy events. Given the expected uncertainty in measured transient  $\Delta W$  of  $\pm 0.9$ kJ, it is entirely possible that there is a critical transient energy above which  $High\ Burn\ Through\ Events$  are occurring and therefore they are linked to a different physics regime.  $\Delta W/P_{gas}$  does not describe the full combined dataset with the full range of peak heat loads although it describes very well the dataset  $<2MW/m^2$ .

A repeat of the divertor gas scan was carried out with nitrogen instead of deuterium fuelling. Each discharge had a constant nitrogen flow rate, leading to a rising nitrogen inventory in the divertor over time. The divertor neutral nitrogen pressure was computed using the DART code [12], which can analyse multiple gas species. Peak values of  $\approx 0.3$ Pa of  $N_2$  pressure are observed in the divertor chamber. Although no  $D_2$  gas puffing is performed in the divertor chamber during these scans, the  $D_2$  source due to plasma exhaust results in  $D_2$  pressures up to  $\approx 1Pa$  at 800ms. Figure 2(b) shows the per sawtooth analysis of 90 individual transients from the  $N_2$  scan. In contrast to the deuterium gas scan, there is little correlation between the peak heat flux and the transient energy (not shown). This suggests that, over the parameter space explored, the dominant effect is nitrogen pressure rather than the magnitude of the transient itself. Figure 2(b) shows a steep decrease in peak heat flux with increasing nitrogen pressure. On a pressure-to-pressure basis, nitrogen appears to mitigate the heat flux by a factor > 20 times more effectively than deuterium. Fulcher T/U measurements similarly indicate the strong mitigation of heat flux with 0.3Pa of nitrogen. No HBEs were observed in the nitrogen dataset. This can be attributed to the lower transient energies ( $\Delta W < 6$  kJ) reached in these discharges. The underlying reason why no higher energy events occurred in the  $N_2$  scan compared to the  $D_2$  is less clear. It may be due to an indirect stabilising effect of higher deuterium pressure on the sawtooth dynamics, which tends to cause large amplitude events later in the discharge or it may simply relate to random variation in sawtooth energy. Future experiments should examine the impact of nitrogen on  $\Delta W > 6$ kJ transients.

#### 3. COMPARISON OF CONVENTIONAL AND SUPER-X DIVERTOR TRANSIENTS

The Super-X divertor is designed to provide improved heat flux mitigation compared to the conventional divertor, due both to favourable geometry (increased poloidal and toriodal flux expansion and target tilting) and favourable physics conditions (operation in a higher neutral pressure regime enhancing volumetric power dissipation across a long connection length). The relationship between heat flux at the target and separatrix power can be summarised, for lower single null discharges, as:

$$q_{\perp} = F_{\text{Geom}} \frac{P_{\text{sep}} f_{\text{out}}}{2\pi \lambda_q} = \frac{\cos \theta_{\text{total}}}{R_{\text{target}} \sin \gamma f_{\text{pol}}} \frac{\Delta W}{\Delta t} \frac{f_{\text{out}}}{2\pi \lambda_q}$$
(1)

where  $f_{out}$  is the fraction of heat flux to the outer divertor excluding effects such as radiation and  $F_{\text{Geom}}$  is

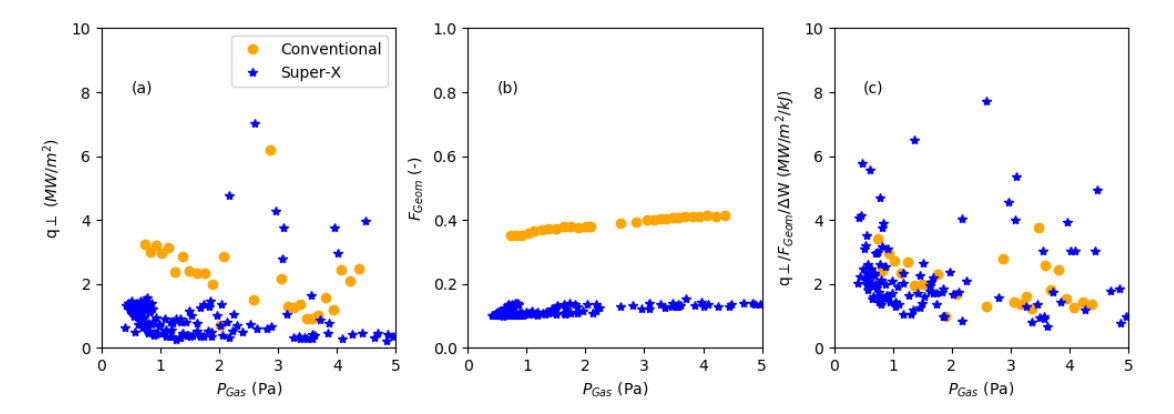


FIG. 3. Analysis of individual sawtooth transients comparing conventional and Super-X divertor discharges. (a) Peak target heat flux vs. divertor neutral gas pressure. (b) Geometry factor  $F_{\text{Geom}}$  determined from equilibrium reconstruction . (c) Peak heat flux normalised by transient energy loss  $\Delta W$ . (d) Peak heat flux further normalised by both  $\Delta W$  and the geometry factor.

a geometry factor that captures the effect of target orientation and magnetic flux expansion. Figure 3 presents a transient-by-transient comparison of two comparable conventional and super-x configuration discharges. Figure 3(a) shows the peak heat flux reached during sawtooth events plotted against divertor neutral pressure; these values are absolute peaks rather than relative changes from the pre-transient baseline. The data in this figure confirm better transient performance in the super-X than in the conventional configuration with the exception of the High Burn Events in the Super-X at  $q_{\perp}$  i2 i2 i2 i2 i2 i3 i4 i5 i5 shows the geometry factor i5 i7 from equilibrium reconstruction. Finally, Fig. 3(c) normalises by both i6 i7 i8 shows the geometry factor i8 from equilibrium reconstruction. Finally, Fig. 3(c) normalises by both i8 i9 i9 shows the geometry factor i9 from equilibrium reconstruction. Finally, Fig. 3(c) normalises by both i9 i9 shows the geometry factor i9 from equilibrium reconstruction. Finally, Fig. 3(c) normalises by both i9 i9 shows the geometry factor i9 from equilibrium reconstruction. Finally, Fig. 3(c) normalises by both i9 shows the geometry factor i9 from equilibrium reconstruction. Finally, Fig. 3(c) normalises by both i9 shows the geometry factor i9 from equilibrium reconstruction. Finally, Fig. 3(c) normalises by both i9 shows the geometry factor i9 from equilibrium reconstruction. Finally, Fig. 3(c) normalises by both i9 shows the geometry factor i9 shows t

# 4. DIVERTOR $T_e$ AND $n_e$ AT HIGH HEAT FLUX

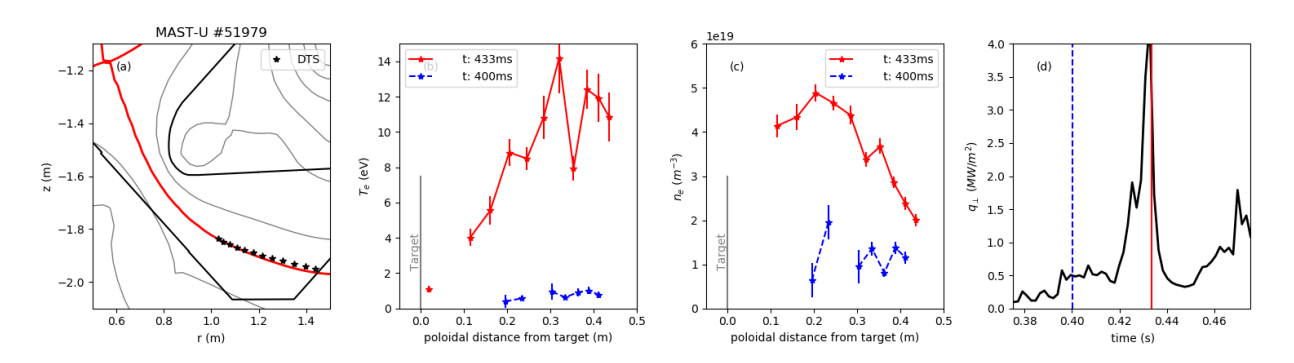


FIG. 4. Profiles obtained during a sawtooth event. Measurements from DTS of (a) contours of magnetic flux showing the last closed flux surface near the target (b) electron temperature and (c) electron density (d) Peak target heat flux from infra-red camera data

The DTS diagnostic was operating over the various gas scans discussed in this paper. One of the sawteeth diagnosed is shown in figure 4. A timeslice from the quiescent period before the sawtooth time is shown for reference. The timings of the profiles relative to the nearest sawtooth event, as indicated by  $q_{\perp}$ , are overlaid with the vertical lines indicating the laser as shown in figure 4(c). For the pulse in the inter-transient period, the temperature is  $\approx 1eV$  (fig 4(b)) and the density shown in (fig 4(c)) falls toward the target. The profiles are typical of a *detached* plasma on MAST-U. UFDS measurements support the indication that this plasma is detached between sawtooth events. The profiles during the sawtooth show elevated temperature up to 8eV 40cm from the target and density rising toward the target. These profiles are indicative of re-attachment during the transient. To determine more generally

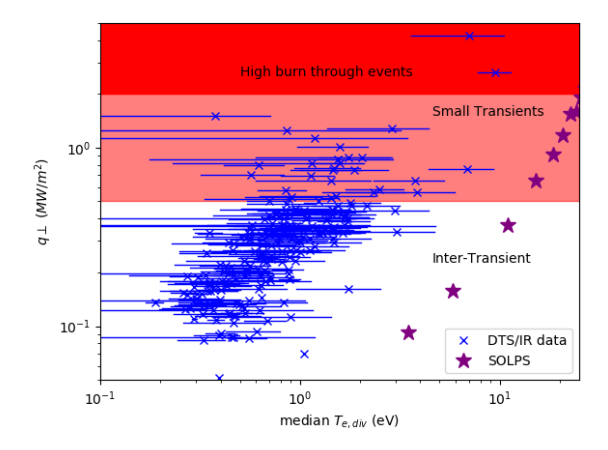


FIG. 5. Target heat flux versus median target electron temperature from 25 MAST-U discharges

the relationship between the peak heat flux in the divertor and the target temperature, data were examined over 25 discharges from 51376-52125. The only criterion for selection of these 25 discharges was that the strike leg was in the super-X configuration, so in contrast to the data examined elsewhere in this paper, this dataset contains varying plasma current and plasma shaping. Additionally, the data are not limited to discharges with fast IR measurements. The data from this scan are shown in figure 5. For each DTS timeslice, the median value of  $T_e$  over the full DTS chord was determined and plotted against the heat flux at that time. The data show the median  $T_{e,div}$  increasing with the heat flux from around 0.5eV up to 10eV. For illustative purposes bands are added corresponding to 1)  $< 0.5 MW/m^2$  which is inter-transient quiescent type heat flux level and typical of  $T_{e,div}$  < 1-2eV 2) small transients  $< 2MW/m^2$  which typically have  $T_e < 6 - 8eV$  and result from transient energy losses of  $\Delta W < \approx 6kJ$  and 3) HBEs which are  $> 2MW/m^2$ , have  $T_e > 8 - 10eV$  and result from transient energy losses of  $\Delta W > \approx 6kJ$ . These data were compared with SOLPS-ITER [13] simulations, also plotted on figure 5, which show similar behaviour but generally indicate higher electron temperature at the target for similar values of heat flux.

## 5. EXHAUST SIMULATIONS

#### 5.1. Reduced 1D multifluid exhaust simulations

Simulations from a multifluid 1D exhaust code written in the ReMKiT1D framework have been performed. The code reintroduces many of the features of the SOL-KiT model [14], with the addition of independent fluid equations and variables for ions as in [15], but retaining purely parallel diffusive neutral transport. Flux expansion is simulated by varying the finite volume cell face area and Jacobian in space. Cells in the upstream 10m (to the x-point) are constant area, which then increases linearly by a factor 4 over the downstream 10m toward the target. Increasing the cell area size means there are more neutrals in that volume for a given density. Global sources and sinks are similar to SOL-KiT. The global energy source is the upstream background heating. The plasma sink is the Bohm (narrow sheath) boundary condition applied at the target cell, where 100% of the incident ion flux  $\vec{\Gamma}_i$  is converted to neutrals that may be ionised back into plasma. There are no global plasma particle sources and the total number of electrons, ions and neutrals is conserved. Neutral temperature in this ReMKiT1D model is fixed at the Franck-Condon dissociation temperature of  $T_n = 3 eV$ , the dissociation of recycled  $D_2$  happens on an imperceptibly fast timescale, and no D<sub>2</sub> molecules are present. Two batches of simulations are conducted to test different recycling "retention times" at the wall. Ions reaching the wall are converted to an inert, immobile species (representing wall ad-/desorption) that spontaneously convert to neutrals after some average time via exponential decay. Here, "instant recycling" refers to a very short average retention time of 10ns, far shorter than the transient events of interest. "Delayed recycling" refers to an average retention time of  $t_{transient}$ , thereby only allowing the release of neutrals from the wall shortly after the transient is deactivated. A consequence of delayed recycling is that there will always be a fraction of the total plasma population that remains wall-embedded, hence the initial plasma inventory must be adjusted for the final equilibria to resemble that of another retention time case. Each batch consists of a scan across initial plasma inventory to obtain two detached plasma equilibria with identical plasma parameters but different recycling retention times. For each equilibrium, a transient heat flux increase to the background heating power is applied. The "transient" is a fixed increase in heating power of duration  $t_{transient} = 1ms$  that is applied either to electrons, ions, or half each to both. A scan of 24 runs per recycling time was performed, including 8 transient energies for each of the 3 lists of transient-heated species.

#### 5.2. Spatial profiles of plasma parameters

Figures 6(a,b,c) respectively show the  $n_e$ ,  $T_e$  and neutral atomic deuterium density  $n_n$  versus the parallel distance x from the target (at x=0) in the rest frame of a SOL flux tube. For each plasma variable: the pre-transient equilibrium and end-of-transient profiles are shown for the two recycling retention times.

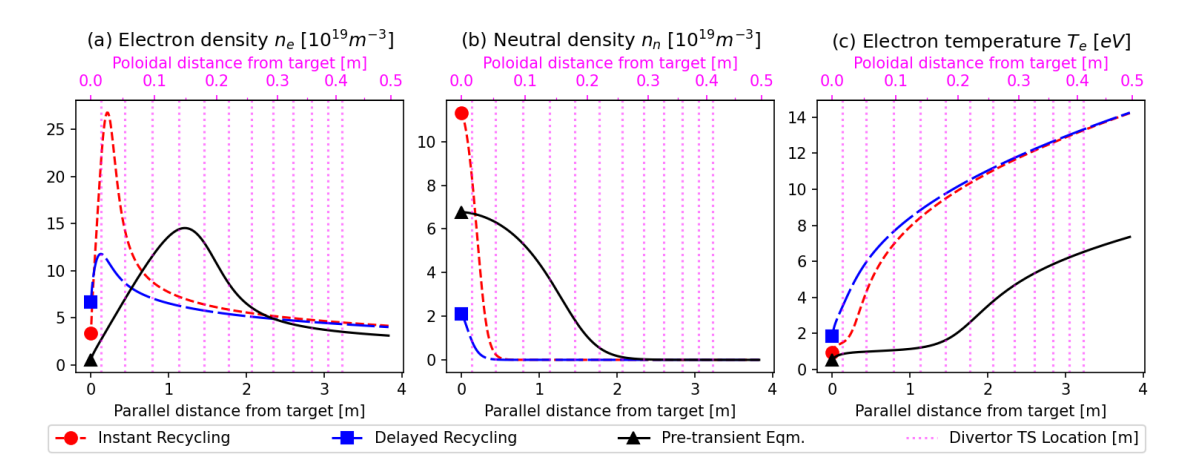


FIG. 6. Simulated parameters before and after an 8 kJ, 1 ms transient for two different ion-target recycling retention times. (a)  $n_e$ , (b) neutral deuteron density  $n_n$ , and (c)  $T_e$ . Each panel shows pre-transient equilibrium (solid black), and the final values with instantaneous ion-target recycling (short dashed red) and delayed recycling (long dashed blue).

Also shown in figure 6 is the estimated poloidal distance from the target, using reconstructed MAST-U field geometry data depicted by the red curve in Figure 4(d). This represents a field geometry that is poloidally aligned with the DTS-UFDS diagnostic sight lines. The plasma density  $n_e$  profiles are shown in figure 6(a). The pre-transient detached equilibrium  $n_e$  profile initially peaks at a parallel distance of x = 1.2m from the target, or an estimated poloidal distance of 0.15m. Post-transient, the peak reaches the target while  $n_e$  at the target (x=0) is increased. In the instant recycling case, the increased ion flux at the target creates neutrals that are readily ionised, adding to the electron density already present there and causing an artificial compression. This feedback loop depletes the plasma of energy once the  $n_e$  peak approaches the target, inhibiting further rises in  $n_e$  and  $T_e$  unless there is a sufficiently high transient energy. Delaying recycling mostly eliminates this artificial compression while the transient is active. Instead, the  $n_e$  peak drops below pre-transient levels and the target  $n_e$  increases to 2 times that of the instant recycling case. Post-transient, the initial flux of ions will release. For the neutral density  $n_n$  in figure 6(b), the bulk of the initial neutral population pre-transient is burned through in both cases except close to the target, where recycling again determines the outcome. Artificial compression causes  $n_n$  at the target in the instant recycling case to increase by nearly 50% rather than decrease by 50% in the delayed recycling case. Because only heating power transients are considered, no new particles are added during the transient (to uphold particle conservation in the absence of other sources/sinks). The  $T_e$  evolution is shown in Figure 6(c). At pre-transient equilibrium,  $T_e$  is flat at  $\lesssim 1 eV$  up to an edge that roughly coincides with the  $n_e$  peak at x=1.2m. Post-transient, the  $T_e$  edge moves to within 0.3mparallel distance from the target. In the delayed recycling case, the post-transient  $T_e$  increase is greater than the instant recycling case and the  $T_e$  floor disappears unlike in the latter. A similar  $T_e \sim 1 eV$  floor appears within the diagnostic data within Figure 4, albeit in a more strongly-detached case where the  $T_e$  floor spans the full 0.4m poloidal distance covered by the diagnostic. Comparing the end-of-transient  $n_e$  profile in figure 6(a) with the experimental observation in Figure 4(b) a number of observation are made. In both model and experiment, the  $n_e$  peak advances closer to the target as the neutrals at the target are ionised during the transient. The simulated pre-transient peak may be narrower due to the lack of perpendicular neutral transport in the ReMKiT1D model. Comparing simulated  $T_e$  with experiment in figure 4(a), the measured  $T_e$  profile is flat over the full poloidal distance pre-transient. This plasma is known to be detached pre-transient where its front lies further from the target than in the simulated case.

#### 5.3. Impact of $\Delta W$ on target parameters

In total 48 simulations were conducted using the reduced model. These comprised 8 transient energies from 1-8kJ (or  $1-8MWm^{-2}$  applied for a 1ms duration). Three different sets of species heated by the transient (electrons only, ions only, and 50% for each), and for the two recycling rates. Figure 7 shows the line-average value of  $n_e$  near the target for each run in the full scan of transient powers  $\Delta W$ , list of species heated by the transient, and recycling time. The line average of each plasma parameter over [19.9m, 20.0m] is roughly the poloidal distance between the

target and the nearest DTS diagnostic measurement position to the target.

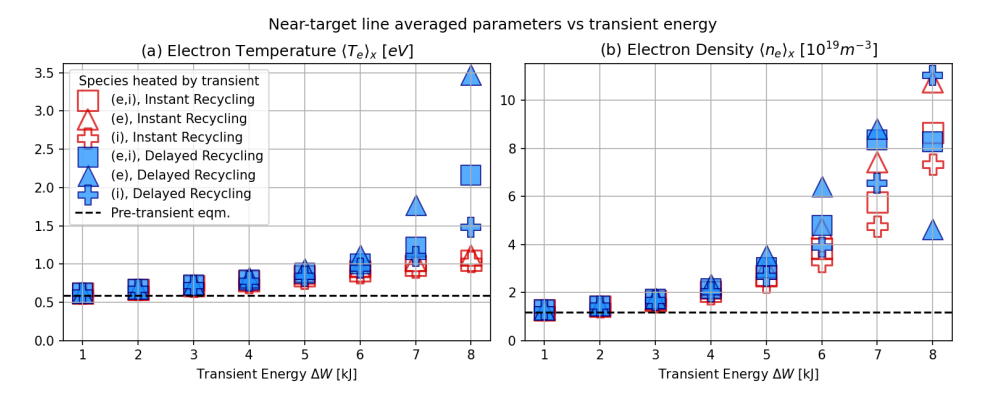


FIG. 7. Target parameters, averaged over parallel distance x = [19.9m, 20.0m], versus transient energy for each list of species heated by transient and each recycling retention time.

Focusing on  $T_e$  in figure 7(a), at lower energies of  $(\Delta W < 4kJ)$ , both recycling cases gave modest post-transient increases in near-target  $n_e$  and  $T_e$  with weak dependence on which species were heated by the transient. This is due to the plasma not having fully burned through the neutral cloud and reaching the target once the transient ceases. For  $\Delta W \gtrsim 5kJ$ ,  $T_e$  for the delayed recycling case then increases significantly, the electron-only heating cases increased most post-transient compared to other species cases. Here, the plasma received enough energy to burn through to the target and is now influenced by recycling. Recalling the profiles in Figure 6, a long recycling wall retention time reduces the neutral population adjacent to the target and the associated plasma energy losses due to collisions, increasing the post-transient  $T_e$  there. The effects of recycling at the higher  $\Delta W$  are species-dependent. In this particular model, only electrons carry out ionisations (ion-neutral ionisation is assumed to be negligibly slow) and therefore a transient that heats electrons only will burn through the most neutrals and would produce the greatest  $T_e$  increase. Heating ions only will delay the transfer of energy to electrons and subject the energy to additional losses until it is transferred (including the Bohm sheath boundary condition). For the  $n_e$  in Figure 7(b), a similar upward trend in  $n_e$  occurs above  $(\Delta W \gtrsim 5kJ)$ , especially in the delayed recycling and electron-heated cases. However, in the delayed recycling case, for the electron-only and electron-ion heating cases,  $n_e$  rises then drops beyond  $\Delta W \gtrsim 7kJ$ , as the plasma peak advances closer to the target before reattaching and draining into the wall. This is unlike the instant recycling case which has an artificially compressed plasma and neutral density at the target, recalling Figures 6(a,b). It is likely that a much higher transient energy would be required to deplete the neutrals under instant recycling and prevent further neutral creation through recombination. Comparing simulation with experiment, the threshold  $\Delta W$  for the ReMKiT1D model cases is higher, primarily due to the higher plasma and neutral density (more neutrals at target to burn through), but the model also does not include cross-field neutral transport or impurities that would increase the threshold  $\Delta W$ . In reality, there exists a population of hot, fast electrons with larger mean free paths than the domain. This would mean the collisional fluid electron model described here is likely overestimating  $T_e$  in the purely electron-heated case, which suggests that if the transient energy and upstream  $T_e$  are sufficiently high, this would have less of an effect in increasing the downstream  $T_e$  and the ion and neutral physics become more important. Non-local kinetic effects is a primary research question for ReMKiT1D and is subject to future work.

# 6. CONCLUSIONS AND FUTURE WORK

Sawtooth transients with energy  $\Delta W < 6~\mathrm{kJ}$  typically produce peak heat loads below  $2~\mathrm{MW/m^2}$  in the Super-X lower single null divertor configuration. These transients can be effectively mitigated by deuterium gas puffing, with peak heat loads decreasing at a rate of approximately  $0.17~\mathrm{MW/m^2/Pa}$ . There is a change in target behaviour where  $\Delta W > 6~\mathrm{kJ}$ , with much higher heat fluxes and  $T_{e,div}$ . This could be because the buffering capacity of the neutral gas pressure in the divertor becomes depleted beyond this point. Methods to extend this research and diagnose larger transients will be explored in future campaigns. Seeding of  $N_2$  gas was found to successfully mitigate heat loads with reduction of  $\approx 4MW/m^2/Pa$ . A comparison of conventional and Super-X divertor configurations during transients demonstrated significantly lower  $q_\perp$  in the Super-X case. This improvement was largely consistent with expectations from geometric considerations. A valuable extension would be to repeat this comparison with  $N_2$  seeding, where the more enclosed geometry of the Super-X divertor may enhance radiative losses and offer improved performance. Fully buffering  $\Delta W > 6~\mathrm{kJ}$  transients with  $D_2$  alone appears challenging, however, the prospect of mitigating High Burn Through Events using  $N_2$  gas remains a promising direction for future investigation.

Burn-through scenarios were simulated in a 1D reduced multifluid model developed using the ReMKiT1D framework to investigate the mechanisms involved. Further work is needed to align the ReMKiT1D simulations with

SOLPS-ITER, which will involve remapping SOLPS-derived plasma backgrounds and fields into the 1D simulations similar to recent work with DIV1D code [16]. Cold diffusive-reactive neutral transport in ReMKiT1D is to be replaced with a fluid model to track neutral pressure, energy and momentum transfer, and their effects on burn-through. Molecular  $D_2$  in ReMKiT1D is also of interest, to account for the important molecular processes in the MAST-U divertor influencing detachment [4]. We find that target recycling physics will be important for any future study of the burn-through energy threshold as this becomes crucial during high burn-through events that lead to interactions immediately upstream of the target. Treatment of the target influences the transition between the attached and detached state, and therefore the required energy for any transient to fully "burn-through". This would motivate the future development of a 1D target model within ReMKiT1D - similar to undertakings with the "FACE" model [17]. Results obtained have shown that delayed recycling matches experiment much better and hence there is a good argument to use this for future modelling in general. There is a possibility that non-local kinetic electron effects related to flux expansion will be implemented in a future version of the ReMKiT1D code. Non-local effects will likely reduce the rate of ionisation (as fast electrons will rarely interact with neutrals) thereby increasing the burn-through input energy threshold. Due to the computational challenge of kinetic simulations, this requires the neutral physics improvements to be verified first in a multi-fluid case.

# Acknowledgements

This work has been part-funded by the EPSRC Energy Programme [grant number EP/W006839/1] and [EP/S022430/1]. To obtain further information on the data and models underlying this paper please contact PublicationsManager@ukaea.uk. The ReMKiT1D framework respositories are hosted on GitHub: https://github.com/ukaea/ReMKiT1D.

#### **REFERENCES**

- [1] A. Loarte and et al. "Characteristics of type I ELM energy and particle losses". In: *Plasma Physics and Controlled Fusion* 45 (2003), pp. 1549–1569.
- [2] J. Harrison and et al. "Overview of the MAST Upgrade Super-X divertor". In: *Nuclear Materials and Energy* 12 (2017), pp. 1072–1076.
- [3] A. Fil et al. "Comparison between MAST-U conventional and Super-X configurations through SOLPS-ITER modelling". In: *Nuclear Fusion* (2022). Accepted manuscript. DOI: 10.1088/1741-4326/ac81d8.
- [4] K. Verhaegh et al. "Spectroscopic investigations of detachment on the MAST Upgrade Super-X divertor". In: *Nuclear Fusion* 63.1 (Dec. 2022), p. 016014. DOI: 10.1088/1741-4326/aca10a.
- [5] G. Federici and et al. "An overview of the EU DEMO power plant concept". In: Fusion Engineering and Design 89 (2014), pp. 882–889.
- [6] S. S. Henderson et al. "An overview of the STEP divertor design and the simple models driving the plasma exhaust scenario". In: *Nuclear Fusion* 65.1 (2025), p. 016033. DOI: 10.1088/1741-4326/ad93e7.
- [7] R. A. Pitts et al. "Physics basis for the first ITER tungsten divertor". In: *Nuclear Materials and Energy* 20 (2019), p. 100696. DOI: 10.1016/j.nme.2019.100696.
- [8] M. Komm et al. In: *Nuclear Fusion* 63.12 (Sept. 2023), p. 126018. DOI: 10.1088/1741-4326/acf4aa.
- [9] Jack Flanagan et al. "ELM buffering in the MAST Upgrade Super-X divertor". Manuscript submitted to Nuclear Fusion. 2025.
- [10] S.S. Henderson et al. "Divertor detachment and reattachment with mixed impurity seeding on ASDEX Upgrade". In: *Nuclear Fusion* 63.8 (July 2023), p. 086024. DOI: 10.1088/1741-4326/ace2d6.
- [11] J. G. Clark et al. "First divertor Thomson scattering measurements on MAST-U". In: *Review of Scientific Instruments* 93.10 (Oct. 2022), p. 103534. ISSN: 0034-6748. DOI: 10.1063/5.0101635.
- [12] S.S. Henderson et al. "Validating reduced models for detachment onset and reattachment times on MAST-U". In: *Nuclear Materials and Energy* 41 (2024), p. 101765. ISSN: 2352-1791. DOI: https://doi.org/10.1016/j.nme.2024.101765.
- [13] S. Wiesen et al. "The new SOLPS-ITER code package". In: *Journal of Nuclear Materials* 463 (2015), pp. 480–484. DOI: 10.1016/j.jnucmat.2014.10.012.
- [14] Stefan Mijin et al. "ReMKiT1D: A framework for building reactive multi-fluid models of the tokamak scrape-off layer with coupled electron kinetics in 1D". In: *Computer Physics Communications* 300 (Apr. 2024), p. 109195. DOI: 10.1016/j.cpc.2024.109195.
- [15] D. Power et al. "Scaling laws for electron kinetic effects in tokamak scrape-off layer plasmas". In: *Nuclear Fusion* 63 (2023), p. 086013. DOI: 10.1088/1741-4326/acdca6.
- [16] G. L. Derks et al. In: *Plasma Physics and Controlled Fusion* 66.5 (May 2024), p. 055004. DOI: 10.1088/1361-6587/ad2e37.
- [17] R. D. Smirnov, J. Guterl, and S. I. Krasheninnikov. "Modeling of Multispecies Dynamics in Fusion-Related Materials with FACE". In: *Fusion Science and Technology* 71.1 (2017). DOI: 10.13182/FST16-125.